Numerical Investigations of an Airfoil in a Nonuniform Stream

F. CHOW,* E. KRAUSE,† C. H. LIU,‡ AND J. MAO§
New York University, New York, N. Y.

The nonlinear differential equation for the flowfield around an airfoil in a two-dimensional nonuniform parallel stream is solved by the finite difference method. The numerical results show that even for a thin airfoil at small angle of attack, the stagnation pressure and the vorticity carried by the streamline passing around the airfoil are significantly different from the corresponding values carried by the undisturbed streamline through the body under the linearized approximation. When the deviation upstream from the uniform flow is represented by a Gaussian profile to simulate the velocity increment behind a propeller, the numerical results show that there is an optimum vertical location of the airfoil relative to the upstream profile for maximum lift. A correlation between the maximum lift and a nonuniformity parameter of the upstream profile is obtained. This parameter is a combination of two parameters, the maximum velocity deviation and the spread of the nonuniformity. When the upstream velocity profile changes from one uniform stream to another through a layer with a steep velocity gradient, there is a significant gain (loss) in lift, if the vorticity is in the same (opposite) sense as the circulation around the wing. A more drastic change in lift occurs, however, when the circulation is in the opposite sense as the vorticity. This occurs when the layer with a steep velocity gradient passes over the upper surface of the airfoil. This phenomenon of a sudden change in lift is of importance when an airplane encounters an atmospheric disturbance.

1. Introduction

IN the studies of the interference effect of propellers on an airfoil,[1,2] it is usually assumed that the disturbance of an airfoil on the jet stream behind the propeller is small, so that the vorticity and stagnation pressure are carried along the streamline of the undisturbed jet. This assumption is essential for the linearization of the problem and makes the analysis manageable. For an evaluation of the validity of this assumption, the nonlinear problem of a two-dimensional airfoil in a nonuniform parallel stream is examined. The nonuniform stream simulates the flow behind the propeller, as shown in Fig. 1. The upstream velocity $U(y)$ is a given function of y and is parallel to the x axis. The governing equation for the incompressible inviscid flowfield is

$$\partial^2\psi/\partial x^2 + \partial^2\psi/\partial y^2 = -\omega(\psi) \tag{1}$$

where ψ is the stream function and ω is the vorticity. $\omega(\psi)$ is a given function of ψ related to the upstream velocity profile, as shown by the following parametric expressions:

$$\omega = -g''(y) = -dU(y)/dy \tag{2a}$$

and

$$\psi = g(y) = \int_0^y U(y)dy \tag{2b}$$

For some special profiles, namely of the linear or exponential type, the nonlinear Eq. (1), becomes the linear equation: $\Delta\psi = C$ or $\Delta\psi = K\psi$, respectively.[2-4]

In order to study the general problem of an airfoil in a nonuniform stream, it is necessary to solve the nonlinear Eq. (1). A numerical program for the solution of the finite difference equation corresponding to Eq. (1) is developed to handle any airfoil shape and any given upstream velocity profile. With this program, several numerical investigations are carried out to shed some light on the effects of displacements of streamlines and the effects of vorticities. It is decided to run "experiments" by means of the computer, rather than in the wind tunnel, not only for economy but also because of the difficulties encountered in generating various upstream velocity profiles in a wind tunnel. The numerical analysis is described in Sec. 2. The numerical results for an airfoil in a nonuniform stream simulating the effect of a propeller are described in Sec. 3. The numerical results for an airfoil in a stream with a large velocity gradient are described in Sec. 4.

2. Numerical Analysis

For an airfoil submerged in a nonuniform stream, as shown in Fig. 1, the vertical location of the airfoil relative to the upstream velocity profile is prescribed. The flowfield obeys the nonlinear differential Eq. (1). Because of the nonlinear vorticity term, the flowfield is rotational and the existing numerical programs[6] for potential flow cannot be employed. The nonlinear dependence of the vorticity ω on the stream function ψ is defined by the upstream velocity profile of Eqs. (2a) and (2b). In Eq. (2b), the stream function ψ at $y = 0$ upstream ($x = -\infty$) is assigned to be zero. The value of the stream function around the airfoil $\psi = C$ is unknown, a priori. If the stream function around the airfoil is set equal to zero, it will then be necessary to change Eq. (2b) to

$$\psi = \int_0^y U(y')dy' - C$$

and the unknown constant C, will appear in the $\omega - \psi$ relationship, and hence, in the differential Eq. (1). With $\omega(\psi)$ defined by Eqs. (2a) and (2b), the unknown constant C will appear only in the boundary condition on the airfoil. For a given upstream velocity profile, given either analytically or graphically as a function of y, a short program is written for Eqs. (2a) and (2b) in which ω is tabulated as functions of ψ, to be used later as input data.

The differential Eq. (1), is reduced to a difference equation for each grid point in Sec. 2.1. For the numerical solu-

Received September 5, 1969; revision received March 3, 1970. This research is supported by the Army Research Office, Durham under Contract No. DA-31-124-ARO-D-464. The authors would like to express their indebtedness to A. Ferri and L. Ting for their supervision.

* Research Scientist, School of Engineering Science.

† Research Scientist, School of Engineering Science; presently at DVL-Institut für Angerwandte Gasdynamik, Porz-Wahn, Germany. Member AIAA.

‡ Assistant Research Scientist, School of Engineering Science.

§ Assistant Research Scientist, School of Engineering Science; presently at Drexel Institute of Technology, Department of Mechanical and Aerospace Engineering.

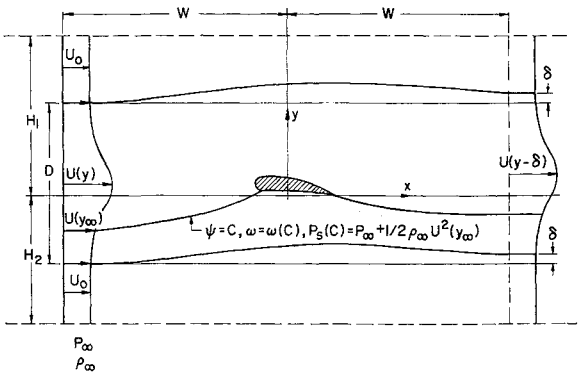

Fig. 1 Airfoil in a nonuniform parallel stream and the boundaries for the finite difference solution.

tion of the difference equation, it is necessary to introduce a finite domain in the shape of a rectangle. The appropriate size and the condition to be imposed on the sides of the rectangle will be discussed. Also, the boundary condition on the airfoil, that is, the value of the stream function $\psi = C$ and the Kutta-Joukowski condition at the trailing edge will be discussed in Sec. 2.2.

2.1 Difference Equation

Instead of setting up a finite difference equation for ψ, it will be done for the disturbance stream function $\bar{\psi}(x,y)$ which is defined as

$$\bar{\psi}(x,y) = \psi(x,y) - g(y) \tag{3}$$

where $g(y)$ is the undisturbed stream function defined by Eq. (2b). The differential equation for $\bar{\psi}$ is

$$\Delta\bar{\psi}(x,y) = -\omega(\bar{\psi} + g) - g''(y) \tag{4}$$

where $-g''(y)$ represents the undisturbed vorticity distribution given by Eq. (2a). Equation (4) holds for $\bar{\psi}(x,y)$ finite or small. The difference Eq. (3) for an interior point (i,j) is[7]

$$\alpha_1\bar{\psi}(i+1,j) + \alpha_2\bar{\psi}(i,j+1) + \alpha_3\bar{\psi}(i-1,j) + \alpha_4\bar{\psi}(i,j-1) - \alpha_5\bar{\psi}(i,j) = -\{\omega[\bar{\psi}(i,j) + g(y_j)] + g''(y_j)\}h^2 \tag{5}$$

The coefficients $\alpha_1,\alpha_2,\ldots,\alpha_5$, are the averaging factors and are related to the distances between the point (i,j) and its four neighboring points as follows:

$$\alpha_1 = 2/[a_1(a_1+a_3)], \qquad \alpha_2 = 2/[a_2(a_2+a_4)]$$

$$\alpha_3 = 2/[a_3(a_3+a_1)], \qquad \alpha_4 = 2/[a_4(a_4+a_2)]$$

and

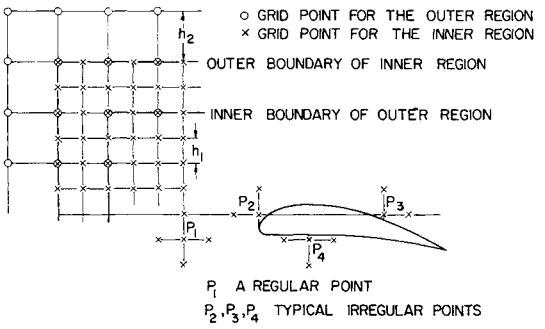

Fig. 2 Regular and irregular points and the overlapping of two regions ($h_2 = 2h_1$).

$$\alpha_5 = 2(a_1a_3 + a_2a_4)/(a_1a_2a_3a_4)$$

where

$$a_1 = (x_{i+1} - x_i)/h, \qquad a_2 = (y_{j+1} - y_j)/h$$

$$a_3 = (x_i - x_{i-1})/h, \qquad a_4 = (y_j - y_{j-1})/h$$

and h is the step size of the regular grid. Most of the interior points are regular points with $a_1 = a_2 = a_3 = a_4 = 1$, $\alpha_1 = \alpha_2 = \alpha_3 = \alpha_4 = 1$, and $\alpha_5 = 4$. Irregular points are located near the airfoil, where one or more of a_1,a_2,a_3,a_4 can be less than unity. The coordinates of all the irregular points and the associated values of a_1,a_2,a_3,a_4 are defined for each airfoil. These are given as input data and are independent of the upstream profile, $U(y)$. Figure 2 shows several irregular points and a regular point.

In order to reduce the total number of grid points, different grid sizes will be used for the regions, with a smaller grid size for the region near the airfoil. Because of the irregular points near the airfoil and the use of different grid sizes, it has been decided to solve the nonlinear difference equation (5) by the simple iteration scheme:

$$\bar{\psi}^{(n)}(i,j) = (1/\alpha_5)\{\alpha_1\bar{\psi}^{(m)}(i+1,j) + \alpha_2\bar{\psi}^{(m)}(i,j+1) + \alpha_3\bar{\psi}^{(m)}(i-1,j) + \alpha_4\bar{\psi}^{(m)}(i,j-1)\} + \{\omega[\bar{\psi}^{(n-1)}(i,j) + g(y_j)] + g''(y_j)\}(h^2/\alpha_5) \tag{6}$$

where the superscripts indicate the number of iterations. One or two of the four m's will be equal to n, while the remaining ones are equal to $n-1$. Their selection will depend on the sequence of the iteration process.

The outer boundary of each region is in the form of a rectangle. The grid size for an outer region is always chosen as an integer multiple of that of the adjacent inner region. These two regions overlap in such a manner that the inner boundary of the outer region lies within the outer boundary of the inner region, by one grid length of the outer region. Figure 3 shows parts of the grid points in a two-region program.

2.2 Boundary Conditions

For the numerical solution of the finite difference Eq. (5), it is necessary to introduce a finite domain and the appropriate boundary condition. For convenience, a rectangular domain of height $H_1 + H_2$ and length $2W$ is chosen, where W is nearly ten times the chord length (Fig. 1). Without the knowledge of the asymptotic behavior of the disturbed stream function $\bar{\psi}$, a simple condition of $\bar{\psi} = 0$ is imposed for a given rectangular region. For the case in which the airfoil is placed inside a wind tunnel, the boundary conditions are $\bar{\psi} = 0$ at $y = H_1$ and at $y = -H_2$. The upstream and downstream conditions of $\bar{\psi} = 0$ at $x = W$ and $x = -W$ become more accurate as W increases. Since an increase in W requires only a linear increase in the number of grid points of the larger grid size, the increments in storage space and in computer time are not excessive. From the numerical results in the next subsection, it is found that the pressure distribution for a given airfoil and upstream profile, $U(y)$, changes by less than 1% when W is doubled. The accuracy of this approximation for an infinite domain will be examined in Sec. 2.3, by comparing the numerical solution for an airfoil in a uniform stream with the exact solution and by comparing the numerical solutions for nonuniform stream with different sizes of domain, i.e., with double width or double length or both.

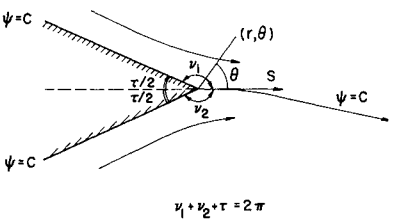

Fig. 3 Equivalent statement of the Kutta-Joukowski condition.

On the surface of the airfoil, the stream function ψ should be equal to a constant C. For each assigned value of C, a numerical solution can be obtained. The correct value for C has to be defined by the Kutta-Joukowski condition at the trailing edge.

For the airfoil in a nonuniform stream, the vorticity near the trailing edge can be approximated by the Taylor series in $\psi - C$, i.e., $\omega(\psi) \sim \omega(C) + (\psi - C)\omega'(C)$. The approximate differential equation is $-\Delta\psi = \omega(C) + (\psi - C)\omega'(C)$. The solution near the trailing edge can be written as a combination of the general potential solution,[8] and the inhomogeneous solution, i.e.,

$$\psi - C \sim c_1 r^{n_1} \sin n_1\theta + \omega(C) r^2 \sin(\theta - \nu_1) \frac{\sin(\theta + \nu_2)}{[2\cos\tau]} \quad (7a)$$

and

$$\psi - C \sim c_2 r^{n_2} \sin n_2\theta + \omega(C) r^2 \sin(\theta - \nu_1) \frac{\sin(\theta + \nu_2)}{[2\cos\tau]} \quad (7b)$$

for $\psi > C$ and $\psi < C$, respectively. With $n_1 = n_2 < 2$, the second terms in Eqs. (7a) and (7b) are of higher order in r and the condition of matching pressure yields $n_1 = n_2$. Therefore, $\nu_1 = \nu_2 = \frac{1}{2}(2\pi - \tau)$.

It is therefore concluded that the Kutta-Joukowski condition is equivalent to the condition:

$$\partial\psi/\partial s = 0 \text{ at the trailing edge} \quad (8)$$

where s is the arc length in the direction bisecting the exterior trailing-edge angle.

For each assigned value C, the solution is obtained and $\partial\psi/\partial s$ at the trailing edge is computed. After three or four trials, a value of C can be obtained to fulfill Eq. (8).

2.3 Accuracy of the Numerical Solution

The errors in the numerical analysis come from two principal sources, the finite grid size and the approximation of an infinite flowfield by a finite domain. These two sources of errors will be examined separately.

To find the proper grid sizes so that the error will be less than a given order of magnitude, numerical calculations for uniform flow around a Joukowski profile at zero angle of attack are performed for a finite domain. The Joukowski profile is obtained from a mapping of radius 0.5 with the center located at $x = -0.05$, $y = 0.05$. The length of the chord is 1.81.

After several numerical experiments, it has been decided to use a rectangle of dimensions 36 × 6.4 as the basic size for the outer region, with a grid size of 0.4, and an inner region of dimensions 4.8 × 4. This combination is considered because in all the check cases an enlargement of the inner region does

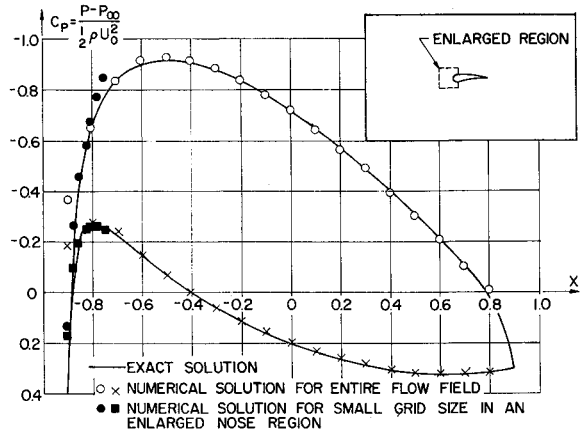

Fig. 4 Airfoil in uniform stream and refined calculation near the nose.

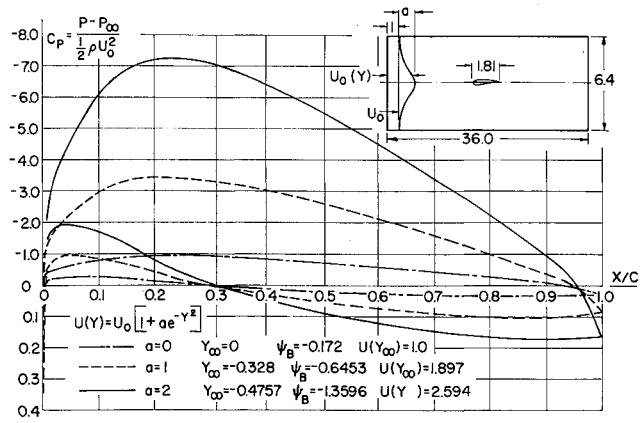

Fig. 5 Pressure distribution on airfoil in stream with various maximum velocities.

not change the accuracy of the pressure distribution on the airfoil. When the exact boundary condition, i.e., the value of ψ given by the analytic solution, is imposed on the boundary of the outer region, the calculation based on a grid size of 0.2 for the inner region yields a difference of nearly 5% in the pressure distribution C_p on the airfoil. With grid size of 0.1 for the inner region, the pressure distribution along the airfoil agrees with that of the exact solution within 1%, except in the nose region where the radius of curvature is of the same order as the grid size (Fig. 4).

To demonstrate that the error near the nose region is a local effect, a finite difference calculation for a local region, 0.4 × 0.4, (Fig. 4), around the nose is carried out. The grid size is reduced to 0.025. On the rectangular boundary, the value of the normal derivative of the stream function given by the numerical solution for the larger flowfield (36 × 6.4) with larger grid size (0.1) is imposed. At the nose, the stream function assumes the same value C as in the larger flowfield calculation. The pressure distribution near the nose given by the finite difference analysis of the local region is in good agreement with the exact solution. This example shows that the finite difference solution for the flowfield around the airfoil of grid size 0.1, nearly $\frac{1}{20}$ of the chord, yields an accurate pressure distribution around the airfoil for the computation of total lift and moment. The result can be used as input data for the boundary condition of a small local region near the nose to obtain a detailed and accurate pressure distribution. It can also be used as a numerical verification of the concept of inner and outer matching in the perturbation solution.[9]

It should be pointed out that a reduction in grid size will improve the resolution and the accuracy of the pressure distribution only if the input data possess enough significant figures. For example, in a numerical calculation for a NACA 4412,[10] profile at 8° angle of attack, the pressure distribution is smooth and within 5% of the exact solution with a grid size $\frac{1}{10}$ of the chord, when the input data for the coordinates of the airfoil and the lengths for the arms of the irregular points are obtained graphically, with accuracy in two significant figures. When the grid size is reduced by half, oscillations in the pressure distribution can be observed. When the grid size is further reduced to $\frac{1}{40}$ of the chord, the oscillation in the pressure distribution is so pronounced that the results become useless. This phenomenon occurs because the percentage error in the lengths of the arms of the irregular points, caused by the inaccuracy in the coordinates of the airfoil, increases as the grid size decreases. This phenomenon can be eliminated by using more significant figures for the coordinates of the airfoil or by computing the coordinates analytically as in the case for the Joukowski airfoil.

From these numerical studies, it is decided that for the inner region, the region around the airfoil, a grid size of $\frac{1}{20}$

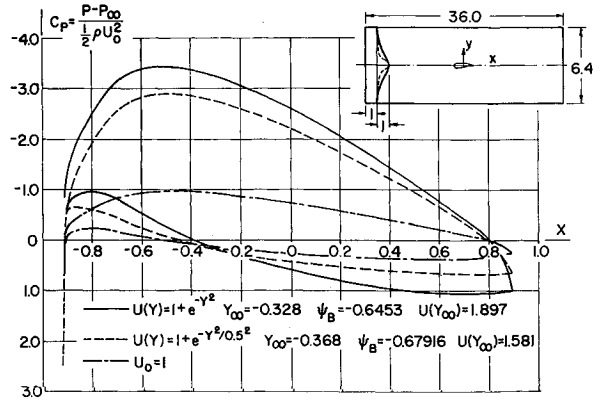

Fig. 6 Pressure distribution on airfoil in streams with various spreads of nonuniformity.

of the chord will be employed to yield good resolution of the pressure distribution with less than 1% error.

In the absence of an exact solution, the simple approximate condition of $\bar{\psi} = 0$ will be imposed on the boundary of the outer region (36 × 6.4). The length of the region is considered satisfactory because the pressure distribution and the total lift will change by less than 1% when the length of the region is doubled. This is true even when the upstream velocity is nonuniform.

Along the top and the bottom of the outer region, the simple boundary condition of $\bar{\psi} = 0$, would simulate two parallel walls. In the case of an airfoil in a uniform stream, the effects of the two walls are of the order of 4% and are in agreement with the theoretical results.[11] For airfoils in nonuniform streams of the types discussed in the next two sections, the simple boundary condition $\bar{\psi} = 0$ can of course be imposed along the top and bottom boundary to simulate wind-tunnel wall effect. When the height of the outer region is doubled, the numerical solution with the same boundary condition $\bar{\psi} = 0$ changes the pressure distribution by 5%. This 5% change due to wall effect is an order of magnitude smaller than those caused by the effects of stagnation pressure and vorticity in the examples presented in Secs. 3 and 4.

For the purpose of demonstrating 1) the dependence of the pressure distribution upon the upstream dynamic pressure and the vorticity carried along the airfoil and 2) the effect on the lift because of relative vertical orientation of the airfoil to the nonuniform stream, all numerical examples presented in the following two sections are carried out for the same Joukowski airfoil at zero angle of attack as described in Sec. 2.3. It is generated by a circle of unit diameter with center located at $x = -0.05$, $y = 0.05$, and is placed near the center of two coaxial rectangular regions. The grid size for the outer region (36 × 6.4) is 0.4 and that for the

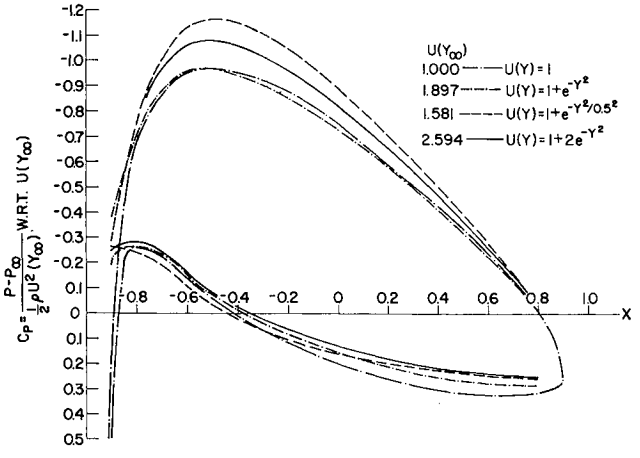

Fig. 7 Comparison of adjusted pressure coefficients.

inner region (4.8 × 4) is 0.1. The simple condition $\bar{\psi} = 0$ is imposed on the boundary of the outer region.

3. Airfoil in a Jet Submerged in a Uniform Stream

For the simulation of a jet submerged in a uniform stream or of a nonuniform stream behind a propeller, the upstream velocity profile is represented by the general type, with three parameters y_s, a, and d,

$$U(y) = 1 + a \exp[-(y - y_s)^2/d^2] \tag{9}$$

y_s represents the vertical orientation of the airfoil relative to the nonuniform stream. Parameter a represents the difference between the maximum velocity and the constant value $U_0(=1)$, and parameter d represents the spread of the velocity nonuniformity. All the length scales are nondimensionalized with respect to the diameter of the mapping circle.

Figure 5 shows the pressure coefficients, with respect to the dynamic pressure of the main stream, i.e., $\frac{1}{2}\rho U_0^2$, for two types of nonuniform stream with the same spread d, i.e., type I, $a = 1$, $d = 1$ and type II, $a = 2$, $d = 1$. For both cases y_s has been set to zero. The pressure coefficient C_p for type I differs from that for a uniform stream ($a = 0$) and even more for type II, the one with a larger maximum velocity.

Figure 6 shows the pressure coefficient for two nonuniform streams with the same maximum velocity but different spread, i.e., type I, $a = 1$, $d = 1$ and type III, $a = 1$, $d = \frac{1}{2}$. Again y_s has been set equal to zero. The pressure coefficient C_p with the larger spread type I differs more from that for a uniform stream ($a = 0$).

The differences in the pressure coefficients are caused by the differences in the upstream dynamic pressure and the vorticity carried by the streamline along the airfoil $\psi_B = C$. To separate these two effects, an adjusted pressure coefficient $\bar{C}_p$ is introduced and is nondimensionalized with respect to the upstream dynamic pressure of the streamline $\psi_B = C$, i.e., $\bar{C}_p = C_p U_0^2/U^2(y_\infty)$.

Figure 7 shows the adjusted $\bar{C}_p$'s for profiles of types I, II, and III. The differences between the adjusted $\bar{C}_p$'s, which are much smaller than those between the regular C_p's, would indicate the effect of vorticity. $\bar{C}_p$ for type I, which has the smallest nonuniformity parameter a/d^2, is almost identical to that for a uniform stream ($a = 0$), i.e., the effect of vorticity is almost nil. However, $\bar{C}_p$ for type III, which has the largest nonuniformity parameter, shows the largest vorticity effect.

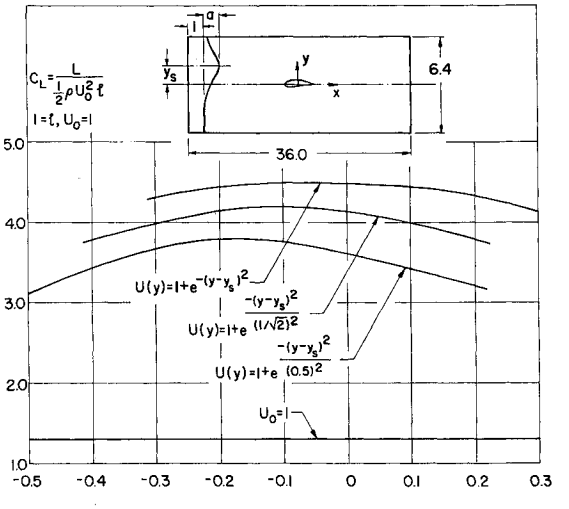

Fig. 8 Optimum location of airfoil to the nonuniform stream

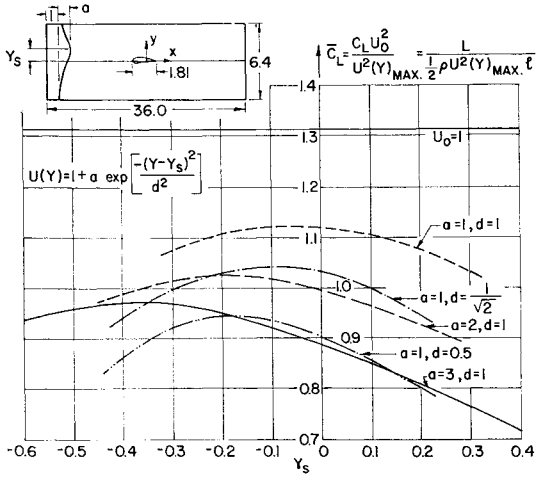

Fig. 9 Comparison of adjusted lift coefficients.

Figure 8 shows the lift coefficient nondimensionalized with respect to the dynamic pressure of the basic uniform stream $\frac{1}{2}\rho U_0^2$ for various values of y_s, and for three types of profiles with the same maximum velocity, i.e., type I, $a = 1$, $d = 1$, type III, $a = 1$, $d = \frac{1}{2}$, and type IV, $a = 1$, $d = 1/(2)^{1/2}$. The optimum y_s's for maximum C_L are negative and $-y_s$ increases as the spread of nonuniformity decreases. The value of maximum C_L, however, decreases as the spread decreases.

Figure 9 shows the variation of lift due to the variations in the three parameters: the relative orientation y_s, the maximum excess velocity a, and the spread d. An adjusted lift coefficient $\bar{C}_L$ is introduced. It is nondimensionalized by the maximum upstream dynamic pressure, i.e., $\bar{C}_L = C_L U_0^2 / U^2(y)_{\max} = C_L(1 + a)^{-2}$. $\bar{C}_L$ agrees with the value $\bar{C}_L{}^*$ for a uniform stream if $a = 0$ or $d = \infty$ or if the nonuniformity parameter a/d^2 is zero. The difference between $\bar{C}_L{}^*$ and the maximum adjusted lift coefficient $\bar{C}_L$ for each type of upstream profile is an indication of the nonuniformity of the stream. The difference increases as the a/d^2 increases. The nonuniformity parameters for type II and type IV are the same, and their maximum $\bar{C}_L$ are nearly the same. This fact suggests the special combination of the two parameters a and d to one parameter a/d^2. Indeed, there is a correlation between the maximum adjusted lift coefficient

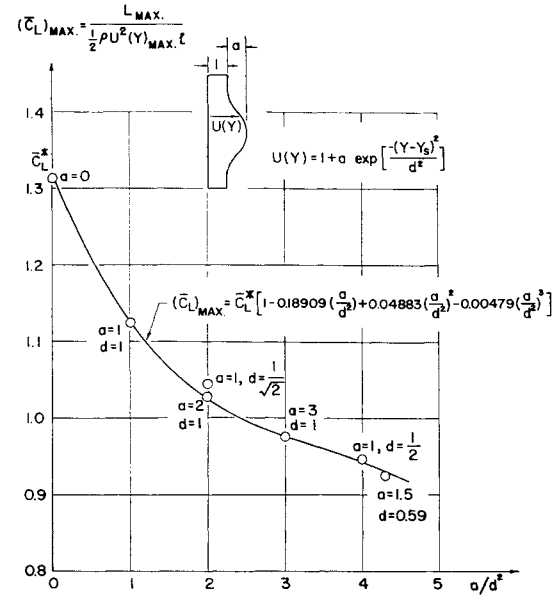

Fig. 10 A correlation between the maximum adjusted lift coefficient $\bar{c}_L$ and the nonuniformity parameter a/d^2.

Fig. 11 An airfoil in a shear layer joining two parallel uniform streams.

$\bar{C}_L$ and the nonuniformity parameter a/d^2 as shown in Fig. 10. Each data point in the figure represents the numerical results for the maximum adjusted lift coefficient $(\bar{C}_L)_{\max}$ at the optimum y_s vs the nonuniformity parameter a/d^2 for each pair of a and d indicated next to the data point. These points, with a ranging from 3 to 0, d ranging from $\frac{1}{2}$ to ∞ and a/d^2 ranging from 0 to 12, lie close to the least square curve given by the equation

$$(\bar{C}_L)_{\max} = \bar{C}_L{}^*[1 - 0.18909(a/d^2) + 0.04883(a/d^2)^2 - 0.00479](a/d^2)^3 \quad (10)$$

When the maximum excess velocity parameter a vanishes or the spread of nonuniformity d becomes infinite or $a/d^2 = 0$, the upstream velocity becomes uniform and $(\bar{C}_L)_{\max} = \bar{C}_L{}^*.(\bar{C}_L)_{\max}$ decreases monotonically as the a/d^2 increases.

4. Airfoil in a Shear Layer between Two Uniform Streams

The problem of an airfoil in a shear layer joining two parallel uniform streams as shown in Fig. 11 may simulate the encounter of an airfoil with atmospheric disturbance. Figure 12a shows the limiting case for two parallel streams with the shear layer degenerated to a vortex sheet along the dividing stream line. Due to the difference in stagnation pressures of the two streams, the dividing stream line cannot intersect the airfoil as shown in Fig. 12b. The airfoil should be either below or above the dividing stream line. If the stream function along the dividing stream line is chosen to be zero, the stream function around the airfoil has to be greater or less than zero. When the position of the airfoil changes upward, the stream function around the airfoil increases from negative to positive, with a discontinuity across zero where there is a sudden change in lift. Since a theoretical analysis for this phenomenon is not yet available, it is expected that the numerical analysis of an airfoil in a shear layer joining two parallel uniform streams will adequately demonstrate the phenomenon as the shear layer thickness diminishes.

For the numerical analysis the upstream velocity profile is chosen to be of the type,

$$U(y) = 1 + a \tanh[(y - y_s)/d] \quad (11)$$

The mean velocity of two uniform streams is used as the velocity scale. The parameter y_s denotes the vertical position of the airfoil relative to the upstream profile, and $2a$ denotes the velocity difference between the two uniform streams. The spread of the shear layer is represented by the positive parameter d. The airfoil is the same Joukowski

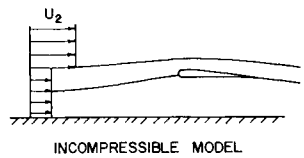

Fig. 12a) Limiting case for two parallel streams with the shear layer degenerated to a vortex sheet along the dividing streamline.

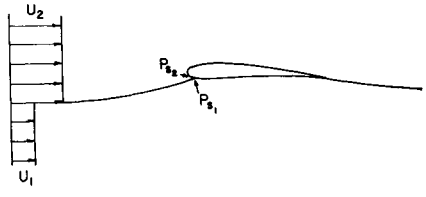

Fig. 12b) Unbalance in pressure at stagnation point.

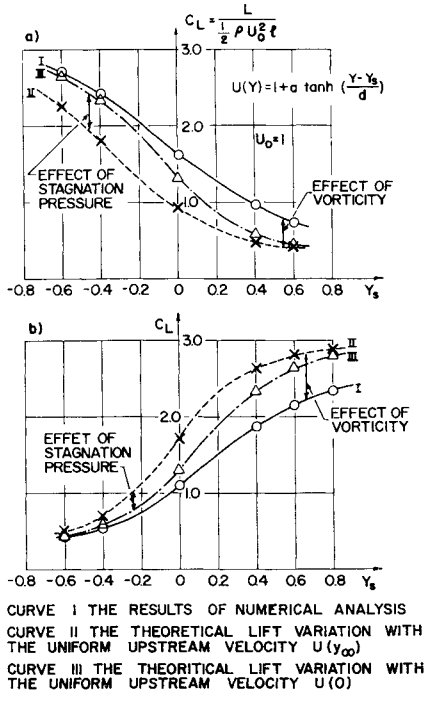

Fig. 13 Lift variation as y_s changes: a) for $a = \frac{1}{2}$, $d = \frac{1}{2}$; b) for $a = -\frac{1}{2}$, $d = \frac{1}{2}$.

profile described in the preceding section and the diameter of the mapping circle is used as the reference length.

Figure 13a shows the lift variation as y_s changes for $a = \frac{1}{2}$ and $d = \frac{1}{2}$. Curve I shows the results of the numerical analysis, yielding the value of the stream function around the airfoil and the corresponding displacement y_∞ of the streamline. Curve II shows the theoretical lift variation with uniform upstream velocity $U(y_\infty)$, i.e., with the same stagnation pressure, as the streamline passes around the airfoil. Curve III shows the theoretical lift variation with the uniform upstream velocity $U(0)$, i.e., with the same stagnation pressure, along the undisturbed streamline $y = 0$ in the sense of linearized theory. Curves II and III include the correction due to wall effect. The difference between curves I and II indicate the effect of vorticity in the nonuniform stream, while the difference between curves II and III show the effect of stagnation pressure due to the upstream displacement of the streamline y_∞. For $a > 0$, the vorticity is in the same sense as the circulation around the airfoil. Therefore, the effect of vorticity increases the lift. The effect of the upstream displacement of the streamline because of circulation tends to bring a streamline with lower stagnation pressure ($y_\infty < 0$) around the airfoil and therefore, counteracts the effect of vorticity. For the case considered, the effect of vorticity dominates that of stagnation pressure as shown in Fig. 13a.

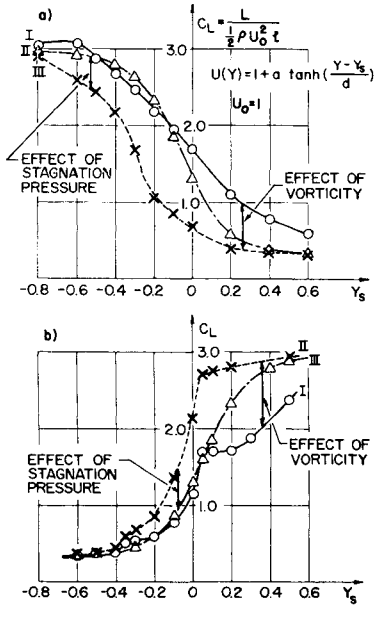

Fig. 14 Lift variation as y_s changes: a) for $a = \frac{1}{2}$, $d = \frac{1}{4}$; b) for $a = -\frac{1}{2}$, $d = \frac{1}{4}$.

Figure 13b shows the lift variation as y_s changes for $a = -\frac{1}{2}$ and $d = \frac{1}{2}$. Again curve I shows the results of numerical analysis and curves II and III have the same meanings as those in Fig. 13a. With $a < 0$, the vorticity is in opposite sense to the circulation around the wing, causing a reduction in lift. On the other hand, the upstream displacement y_∞ of the streamline passing around the airfoil is always in the opposite sense to the circulation, and therefore increases the stagnation pressure and yields an increment in lift. Again the effect of vorticity dominates that of stagnation pressure, as shown in Fig. 13b. Since the upstream velocity profile in Fig. 13b is a mirror image of that in Fig. 13a, with respect to the axis $y_s = 0$, curve III in Fig. 13b and that in Fig. 13a have the same property. However, the mage of the actual lift variation, curve I, in Fig. 13b is below that of curve III, which in turn is below curve I in Fig. 13a. This is because of the change of sign of vorticity in the shear layers with respect to the circulation.

Figure 14a shows the lift variation as y_s changes for a thinner shear layer with vorticity in the same sense as the circulation around the airfoil ($a = \frac{1}{2}$, $d = \frac{1}{4}$). Qualitatively, these three curves I, II, and III are similar to those in Fig. 13a; there is a steepening of the lift variation because of the decrease in the effective thickness d of the shear layer.

Figure 14b shows the lift variation curves for a thin shear layer with vorticity in the opposite sense as the circulation around the airfoil ($a = -\frac{1}{2}$, $d = \frac{1}{4}$). It is quite evident that there is a sudden change of lift near $y_s = 0$. Figure 15 shows the same lift variation vs y_s from the numerical analysis, curve I, and also the curves for corresponding variations in the upstream vorticity $\omega(y_\infty)$, and the upstream displacement y_∞ of the streamline passing around the airfoil. The sudden change in lift, which is accompanied by a sudden change in y_∞, occurs when the vorticity begins to rise from zero, i.e., where the main part of the shear layer is passing over the upper surface of the airfoil. There is an additional sudden drop of lift, but much smaller in magnitude, when the vorticity returns to zero as the shear layer is passing below the lower surface. This sudden change in the upstream displacement of the streamline passing around the airfoil clearly demonstrates the phenomenon mentioned before for the limiting case of $d = 0$ (Fig. 12a). When the vorticity is in the same sense as the circulation (Fig. 14a) the lift variation curve is steeper than that with double thickness in shear layer (Fig. 13a). However, the phenomenon of a sudden jump in lift as shown in Fig. 13b is still absent.

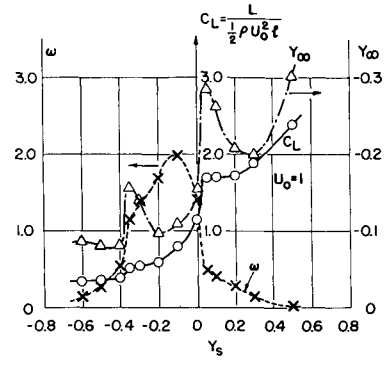

Fig. 15 Lift variation vs y_∞ for $a = -\frac{1}{2}$ and $d = \frac{1}{4}$ from the numerical analysis and the corresponding variations in the upstream vorticity $\omega(y_\infty)$, and the upstream displacement y_∞ of the streamline passing around the body.

5. Conclusions

A numerical program for the finite difference solution of the incompressible flowfield around an airfoil in a two dimensional nonuniform stream is developed. It is employed to obtain the pressure distribution on a thin Joukowski airfoil with small effective angle of attack in a nonuniform stream. Two general types of nonuniform streams are investigated, namely a jet in a uniform stream (Sec. 3) and in a shear layer joining two uniform streams (Sec. 4).

The numerical results demonstrate strong interaction between the vorticity in the nonuniform stream and the circulation around the airfoil, and that between the stagnation pressure carried along the streamline passing around the airfoil and the circulation. The changes in pressure distribution due to the vorticity and stagnation pressure effects are much more pronounced on the upper surface than those on the lower surface (see Figs. 5–7).

When the upstream velocity deviation from a uniform flow is represented by a Gaussian profile to simulate the velocity increment because of the jet or that behind a propeller, the numerical results show that there is an optimum vertical location of the airfoil relative to the upstream profile for maximum lift. A correlation between the maximum lift and a nonuniformity parameter of the upstream profile is obtained. This parameter is a combination of two parameters, the maximum deviation in velocity a and the spread of the nonuniformity d.

When the upstream velocity profile changes from one uniform stream to another through a layer with a steep velocity gradient, the upstream vorticity $(-dU/dy)$ has the same sign as the circulation around the wing. The numerical results show that there is a gain (loss) in lift if the vorticity is in the same (opposite) sense with the circulation around the wing. The upstream displacement y_∞ of the streamline passing around the airfoil is in opposite sense to the circulation, i.e., $y_\infty < 0$. There is a gain (loss) in stagnation pressure along that streamline if $dU/dy < 0$ (>0). The effect of the stagnation pressure, therefore, counteracts that of vorticity but the latter dominates the former. When the main portion of the layer with a steep velocity gradient is passing above the airfoil their difference is significant.

As the velocity profile in the shear layer steepens, the lift variation as a function of the vertical position (y_∞) of the airfoil relative to the upstream profile, will likewise steepen. With the vorticity in opposite sense to the circulation, a sharp change in lift occurs when the layer with large vorticity is passing over the upper surface of the wing, as shown in Fig. 14b with $a = -\frac{1}{2}$, $d = \frac{1}{4}$. When the sign of vorticity is reversed ($a = \frac{1}{2}$, $d = \frac{1}{4}$), such a sudden jump in lift is absent (Fig. 14a). This fact suggests that for a given upstream velocity profile, an airfoil which induces a circulation in the same sense as the upstream vorticity, produces a more gradual change in aerodynamic force than that with a circulation in the opposite sense. Attempts should be made to confirm the results of present numerical investigations by experiments and to understand them better by theoretical analysis.

References

[1] Ferrari, C., "Propeller and Wing Interactions at Subsonic Speeds," *Aerodynamic Components of Aircraft at High Speed*, edited by A. F. Donovan and H. R. Lawrence, Sec. C, Princeton University Press, Princeton, N. J., 1957, Chap. 3.

[2] Cumberbatch, E., "A Lifting Surface Theory for Wings at High Angles of Attack Extending Through Multiple Jets," AD-423274, July 1963, Vehicle Research Corp., Pasadena, Calif.

[3] Tsien, H. S., "Symmetric Joukowski Airfoils in Shear Flow," *Quarterly of Applied Mathematics*, Vol. 1, No. 2, 1943, pp. 130–148.

[4] Murray, J. D. and Mitchell, A. R., "Flow with Variable Shear Past Circular Cylinders," *Quarterly Journal of Mechanics and Applied Mathematics*, Vol. X, Pt. 1, 1957, pp. 13–23.

[5] Jones, E. E., "The Elliptic Cylinder in a Shear Flow with Hyperbolic Velocity Profile," *Quarterly Journal of Mechanics and Applied Mathematics*, Vol. XII, Pt. 2, 1959, pp. 191–210.

[6] Giesing, J. P., "Extension of the Douglas Neuman Program to Problems of Lifting," Infinite Cascades, AD-605207, July 1964, Douglas Aircraft Co., Long Beach, Calif.

[7] Forsyth, G. E. and Mason, W. R., *Finite Difference Methods for Partial Differential Equations*, Wiley, New York, 1960.

[8] Milne-Thomson, L. M., *Theoretical Hydrodynamics*, 3rd ed., MacMillan, New York, 1955.

[9] Van Dyke, M. D., *Perturbation Methods in Fluid Mechanics*, Academic Press, New York, 1964.

[10] Abbott, I. H. and van Doenhoff, A. E., *Theory of Wing Sections*, Dover, New York, 1959.

[11] Thwaites, B., *Incompressible Aerodynamics*, Oxford University Press, New York, 1960.